Chalcogenide Letters Vol. 20, No. 3, March 2023, p. 205 - 213

Determining the majority charge carrier, optical and structural properties of electrochemically deposited lead tin sulfide (PbSnS) thin films

I. Nkrumah*, F. K. Ampong, A. Britwum, M. Paal, B. Kwakye-Awuah,
R. K. Nkum, F. Boakye
Department of Physics, Kwame Nkrumah University of Science and Technology, Kumasi, Ghana

Single phase lead tin sulfide (PbSnS) thin films have been successfully deposited on ITO-coated glass substrates using a 3-electrode electrochemical cell having graphite as the counter electrode and Ag/AgCl as the reference electrode. In this single-step electrodeposition, the PbSnS precursor thin film was directly electrodeposited on the conductive substrate from the electrolytic bath solution which contained $Pb(NO_3)_2$, $SnCl_2.2H_2O$ and $Na_2S_2O_3$. This was followed by annealing in air at 250 °C for an hour to improve the crystallinity. The annealed films were characterized by a variety of techniques. Powder X-ray diffraction revealed peaks which were indexed to the orthorhombic phase of PbSnS with preferred orientation along the (112) plane. Seebeck coefficient studies confirmed the type of charge carrier of the film. SEM micrographs showed a compact morphology composed of spherically shaped well defined grains covering the entire substrate. EDAX analysis of the film was consistent with the formation of PbSnS. Optical absorption measurements revealed the existence of a direct transition with an estimated band gap of 1.68 eV

(Received December 7, 2022; Accepted March 10, 2023)

Keywords: Lead tin sulfide thin films, Electrodeposition, Charge carrier, Solar cell materials

1. Introduction

One of the greatest challenges of our time is to find inexpensive, widely-available, clean and safe alternatives to fossil and nuclear fuels which have finite reserves and adverse consequences on our environment. Solar energy fits this bill and is widely expected to continue, combined with other renewable energy sources, to replace non-renewable energy sources. However, the wide spread applications of solar cells will require dramatic decrease in cost through the use of materials that are promising, environmentally friendly and economical to replace conventional materials [1]. In recent times, the attention of researchers is focused on the large family of chalcogenides that possess very unique and interesting properties. PbS (band gap 0.37 eV) and SnS (band gap 1.3 eV) are two of such chalcogenide compounds which have been extensively studied by many research groups, with a view to reduce the cost of device production [2]. These promising materials find applications in photovoltaic, infrared detection and other opto-electronic devices. There are also available reports which mention $PbSnS_2$ mixed crystals, which can be formed as a result of the high miscibility of the two binary compounds PbS and SnS [3]. These mixed thin film structures have generated significant interest because they offer the advantage of tunable optical and optoelectronic properties. They are useful for the fabrication of devices with predetermined characteristics [4]. Parameters such as band gap, lattice constant and optical absorption and others are varied as a result of mixed thin films of PbS and SnS and results in band gaps of 0.4 to 1.32 eV [5]. These parameters also make them suitable for applications such as solar cell, photochemical, lasers and thermoelectricity [6, 7].

A report by Kuku and Azi [8] on the optical properties of thermally evaporated $PbSnS_3$ thin films, suggests that this material has an optical band gap which makes it attractive for possible

* Corresponding author: inkrumah.sci@knust.edu.gh
https://doi.org/10.15251/CL.2023.203.205

photovoltaic applications. Lately, it has been demonstrated that $PbSnS_2$ can be utilized as a part of thermoelectric composite material, collectively with PbTe [2].

$PbSnS_2$ crystallizes in orthorhombic structure (Pnma space group) [3]. The constituent elements are Earth abundant and due to its vast unexplored potential, Łapińska et al.[3] described it as an unrevealed ternary compound.

Numerous methods such as spray pyrolysis [9], thermal evaporation [8], hot wall vacuum deposition [10], hot-wall epitaxy [11], chemical bath deposition [2, 12, 13] and successive ionic layer adsorption and reaction (SILAR) [14], have been used to synthesize PbSnS. However, there are relatively very few publications on the deposition of the ternary PbSnS by electrochemical deposition.

Production of thin film semiconductors for photovoltaics using electrodeposition gives several advantages when compared to other methods. The technique is simple, has low material wastage, low operating temperature, and relatively low cost apparatus, making it economical. One also has the ability to control film thickness, composition, morphology, etc. by mainly controlling electrical parameters such as electrode voltage and current density, which are easily adjustable. Electrodeposition has emerged as one of the versatile and cost-effective growth technique of metal, metalloid and semiconductor materials [15].

Thin films are very sensitive to the deposition conditions and slight changes can influence the carrier type. For instance, SnS usually occurs as p-type material with layered orthorhombic crystal structure [16]. Doping, annealing effect, excess presence of tin are expected to produce polarity change of SnS to n-type [17]. PbS also exhibits either n-type or p-type semiconductivity depending on the sulfur content.

The type of charge carrier is easily determined by measuring the Seebeck coefficient (S), which is the direct solid state conversion of thermal energy to electrical [18]. The Seebeck coefficient is defined as:

$$S = \Delta V / \Delta T \tag{1}$$

where ΔV is the electric potential difference or the generated thermovoltage created by a temperature gradient, ΔT. The Seebeck coefficient is an intrinsic material property related to the electronic properties, and it is positive for p-type and negative for n-type semiconductors [19]. Several authors including Tzounis et al. [18], Zhang et al. [19], Barrios-Salgado et al. [20] and Kumar et al. [21], have used the Seebeck coefficient to determine the type of carrier in various materials.

In this paper, the ternary PbSnS thin films are produced by direct compound electrochemical deposition. Post deposition annealing is also carried out to improve the crystallinity. The structure, morphology and optical properties of the annealed films are investigated. Seebeck coefficient studies are also carried out to confirm the type of charge carrier of the film. To the best of our knowledge, such a study has not been carried out on PbSnS films produced by the deposition technique employed in this work

2. Methodology

2.1. Substrate preparation

Indium-doped tin oxide (ITO) glass slides with dimensions, 1.2 cm x 4.0 cm, was used as the substrate. The substrates were cleaned in acetone and then rinsed with deionized water. They were then transferred into a beaker containing ethanol and sonicated for 5 minutes after which they were rinsed with deionized water and placed in a desiccator to dry.

2.2. Electrodeposition of PbSnS

The electrolyte was prepared from an aqueous mixture containing lead (II) nitrate, $Pb(NO_3)_2$, as the source of Pb ions, tin (II) chloride dehydrate, $SnCl_2.2H_2O$ as the source of Sn ions and sodium thiosulphate (anhydrous) $Na_2S_2O_3$ as a sulphur source. H_2SO_4 was used to adjust the pH of the electrolyte solution.

The electrolyte mixture contained equal volumes (~30 mL) of 0.003 M $Pb(NO_3)_2$, 0.003 M $SnCl_2.2H_2O$ and 0.1 M $Na_2S_2O_3$ were mixed together in a 100 ml beaker. The pH was adjusted 2.8 by adding a few drops of 2.0 M H_2SO_4, this was done to improve the adherence of the electrodeposits. The concentrations and volumes of electrolytes used were employed to achieve a composition of $Pb_{0.5}Sn_{0.5}S$. Solution purge of dissolved oxygen with argon gas for 10 mins

A conventional three-electrode electrochemical cell was used with ITO-coated glass substrates as the working electrode, graphite as the counter electrode and Ag/AgCl as the reference electrode. Electrodeposition was carried out using an Edaq ER 467 Potentiostat, at a constant potential of -1.3 V vs Ag/AgCl at room temperature (28 °C). A growth time of ~12 minutes was ensured during electrodeposition. The films were deposited by direct compound deposition. After deposition, the films were annealed in air at a temperature of 250 ^oC for an hour before characterization.

2.3. Determination of carrier type

The type of carrier was determined by measuring the Seebeck coefficient (S), using techniques described in Zhang et al. [19].

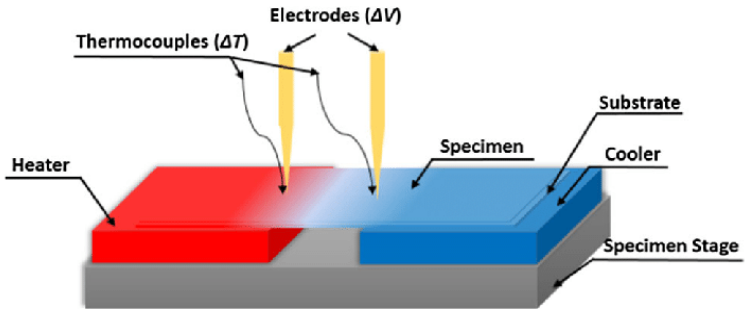

Fig. 1. Schematic diagram of experimental set-up for Seebeck coefficient measurement by Zhang et al. [19].

Using this technique, as shown in Figure 1, one side of the specimen was heated, whilst the other side placed on the cooler to build the temperature difference, ΔT, along the specimen. The temperature was measured by an infrared thermometer, model: YHKY-2000. The induced thermal voltage, ΔV, was measured by a highly sensitive voltmeter, (PeakTech. DMM/LCR METER 2180).

2.4. Thin film characterization

Optical absorption spectra were recorded with a Cecil CE7500 series double beam UV-Visible spectrometer operating in the wavelength range of 190 nm to 1100 nm, a step height of 0.3 nm and a scan rate of 5nm per second, at room temperature. X-ray diffraction studies were performed using a PANalytical Empyrean Series 2 powder X-ray diffractometer with a Cu-kα radiation (1.5406 Å) in the 2θ range 10 to 90. The machine was operated at 40 mA and 45 kV for phase analysis using the Bragg-Brentano geometry. Total analysis time per samples was around 35 minutes for a 2θ scan step of 0.06°. XRD data treatment and analysis were carried out using high score plus software packages. The elemental composition of the samples was determined using a Phenom instrument with nominal electron beam voltages of 15 kV, attached to the scanning electron microscope.

3. Results and discussion

3.1. X-Ray diffraction studies

The X-ray diffraction (XRD) patterns of the PbSnS film deposited on ITO glass substrate is shown in figure 2. It is worth mentioning that discernable peaks were only observed after annealing in air at 250 ^{o}C for an hour.

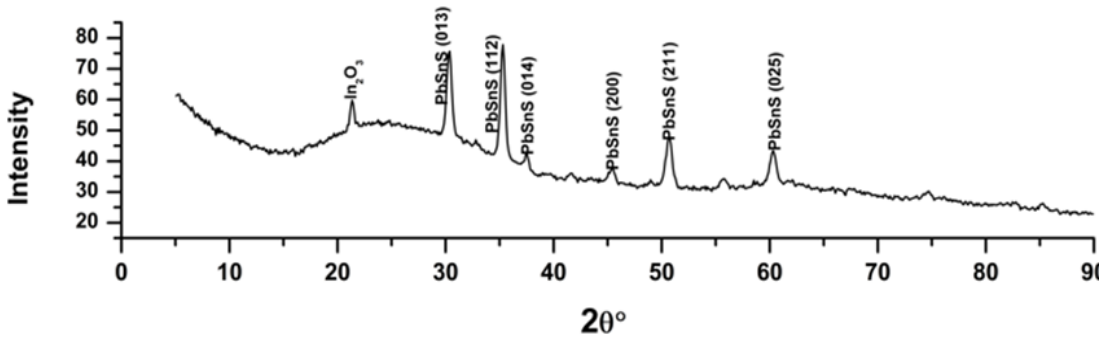

Fig. 2 XRD pattern of the PbSnS film deposited on ITO glass substrate annealed in air at 250 ^{o}C for an hour.

The pattern of prominent peaks in the diffractogram in figure 2, were matched to the orthorhombic phase of PbSnS (Ref.Code. 98-015-6131). The absence of any impurity peaks is a clear indication of the high purity of the sample. Other authors, employing different deposition techniques, have made observations which are in contrast to what has been reported in this work. For instance, Damisa et al. [22], reporting on the structure of electrochemically deposited PbSnS thin films, observed, a mixture of several phases comprising the orthorhombic Sn_2S_3, hexagonal SnS_2 and cubic structure PbS.

The pattern list in Table 1, confirms the chemical formula of the PbSnS film deposited as $Pb_{0.5}Sn_{0.5}S$. The presence of Diindium Trioxide and Indium Tin Oxide in the pattern list may emanate from the substrate. Thus we can conclude that the deposition conditions used in this work, produced a pure and single phase PbSnS thin film.

3.1.1. Average grain size

Calculation of the average grain size from the most intense peak was done using the Scherrer [23, 24] formula which is given as;

$$D = \frac{K\lambda}{\beta \cos\theta} \tag{2}$$

where $\boldsymbol{D}$ is the average grain size, λ is the X-ray wavelength, (0.15418 nm), β full width at half maximum (FWHM) or integral breadth, of the (112) peak and θ is the corresponding Bragg angle and K is the Scherrer constant. The average grain size is about 12 nm.

Table 1. Shows the pattern list produced from the Diffraction analysis.

Visible	Ref.Code	Score	Compound Name	Displ.[°2θ]	Scale Fac.	Chem. Formula
*	98-016-9420	36	Diindium Trioxide	0.000	0.887	$In_2 O_3$
*	98-005-0849	33	Indium Tin Oxide (1.88/0.12/3)	0.000	0.777	$In_{1.88}O_3$ $Sn_{0.12}$
*	98-015-6131	21	Lead Tin Sulfide (0.5/0.5/1)	0.000	0.174	$Pb_{0.5}S_1Sn_{0.5}$

3.1.2. Determination of majority charge carrier

Measurement of temperature difference, ΔT, along the specimen against the induced thermal voltage, ΔV, yielded the following results shown in Table 2

Table 2. Temperature difference versus induced thermal voltage of the films.

Temperature gradient, ΔT (K)	**Potential difference, ΔV, (mV)**
24.0	0.3
32.3	0.4
35.9	0.5
38.7	0.5

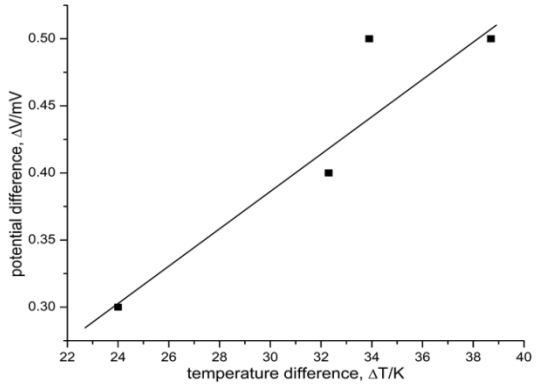

Fig. 3. The induced potential difference ΔV, plotted as a function of temperature difference ΔT.

The potential difference, ΔV, as a function of temperature difference ΔT, gave a straight line and the slope is the Seebeck coefficient. The type of carrier is evident from the temperature dependence of Seebeck coefficient of the films, shown in figure 3. A positive Seebeck coefficient, is indicative of p-type conduction.

3.2. Scanning electron microscopy

Figures 4 to 6 show the SEM micrographs of the PbSnS film taken at different magnifications

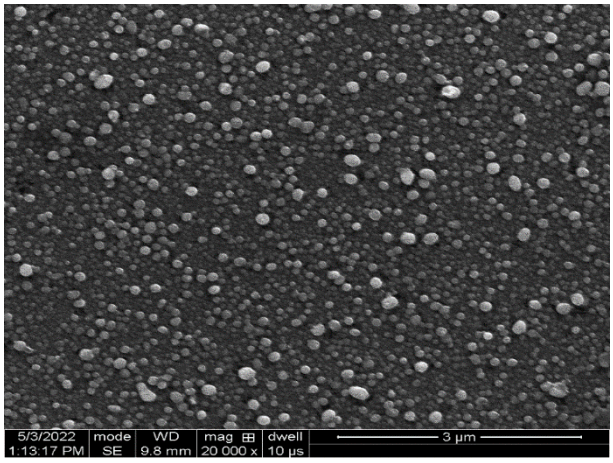

Fig. 4. SEM Micrograph of PbSnS film on ITO glass substrate (magnification 20,000x).

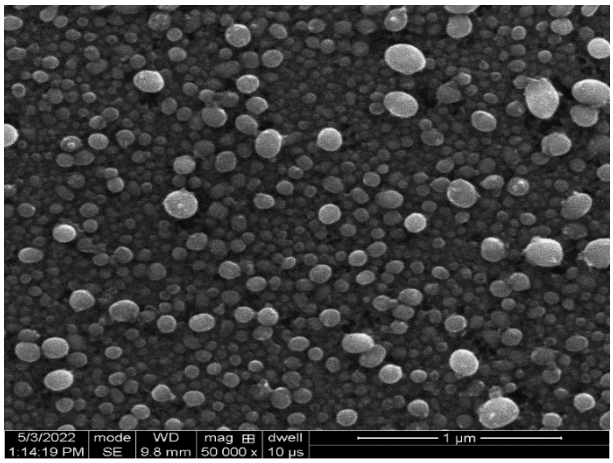

Fig. 5. SEM Micrograph of PbSnS film on ITO glass substrate (magnification 50,000x).

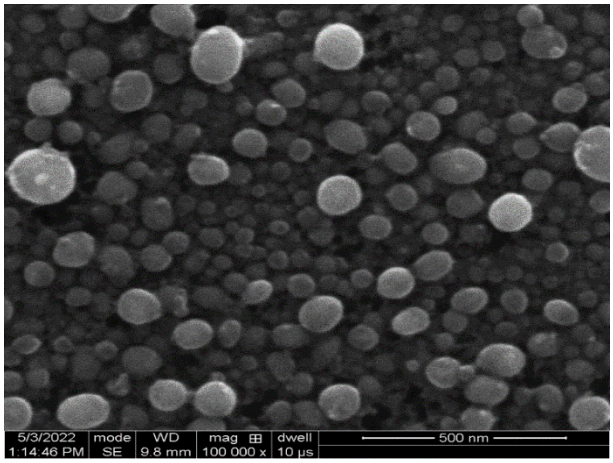

Fig. 6. SEM Micrograph of PbSnS film on ITO glass substrate (magnification 100,000x).

All the SEM micrographs show spherically shaped grains of different sizes, uniformly spread over the entire substrate with no visible holes or cracks. This type of morphology is very

characteristic of films deposited by solution based techniques. The absence of cracks and pinholes are acceptable features for photovoltaic application.

3.3. Energy dispersive x-ray analysis (EDAX)

The EDAX spectrum of the film, shown in Figure 7, is consistent with the formation of PbSnS on ITO glass substrate. The presence of the large amount of silicon, emanate from the ITO glass slide used as the substrate.

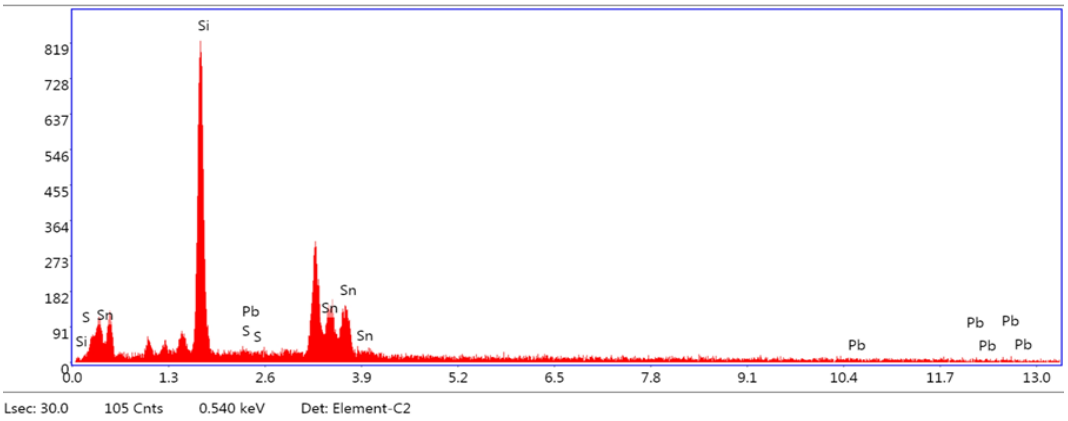

Fig. 7. EDAX spectrum of PbSnS film deposited on ITO glass substrate.

3.4. Determination of the optical band gap

The Energy band gap and type of electronic transition was estimated using the Stern equation [25]. Given as

$$A = \frac{[K(h\nu - E_g]^{n/2}}{h\nu} \tag{3}$$

where v is the frequency, h is the Planck's constant, k equals a constant while the value of n is either 1 for direct transitions and 4 for indirect transitions, respectively. Since PbS and SnS have direct transitions, it follows that their mixed compositions are also direct transitions, hence, n = 1. The band gap energy is obtained by plotting a line of best fit on the $(Ahv)^{2/n}$ versus hv *graph* and extrapolating the line to intersect the energy axis at $(Ahv)^{2/n} = 0$.

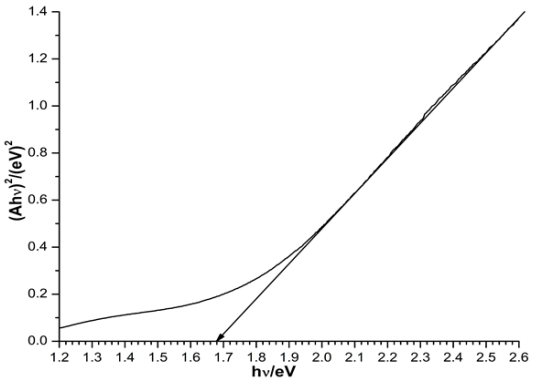

Fig. 8. A plot of (Ahv)² vs hv for PbSnS thin film.

Figure 8 shows the band gap of the PbSnS thin film. Generally, band gap energy in semiconducting materials is mostly influenced by their structural defects, crystallinity, impurities,

grain sizes as well as grain boundary disorders [22]. Figure 8, reveals that the samples have direct band transition with an estimated band gap of 1.68 eV. This value compares favorably well with reports by Sebastian et al. [26], who reported a band gap range of 1.60 to 1.90 eV for lead doped tin sulphide (SnS:Pb) thin films grown by varying lead concentration using Nebulized spray pyrolysis (NSP) technique and Orimi et al. [27] who estimated an optical band gap of 1.63 to 1.80 eV for $Pb_{1-x}Sn_xS$ nano-powder using chemical precipitate technique. A lower band gap range between 1.52 – 1.54 eV reported by Damisa et al. [22] on the electrochemical deposition of PbSnS thin films was attributed to the presence of impurities. Consequently, the band gap value obtained in this work is as a result of the purity of this sample as indicated from the XRD studies.

4. Conclusion

A pure and single-phase PbSnS thin film has been successfully deposited on ITO-coated glass substrates using a 3-electrode electrochemical cell. This was followed by annealing to improve the crystallinity. The preparative conditions were optimized in order to obtain high-quality and well-reproducible PbSnS thin films. X-ray diffraction analyses of the annealed films revealed the orthorhombic phase of PbSnS with preferred orientation along the (112) plane. The average grain size was 12 nm. SEM micrographs showed a compact morphology composed of well-defined spherically shaped grains covering the entire substrate with no cracks or pinholes. EDAX analysis of the film was consistent with the formation of PbSnS. Seebeck coefficient measurements of the films was indicative of p-type conduction. Optical absorption measurements revealed the existence of a direct transition with an estimated band gap of 1.68 eV. The deposition conditions used in this work, produced a pure and single-phase PbSnS thin film, with p-type conductivity and suitable band gap, conducive for photovoltaic applications.

References

[1] J. Fang, D. D. Mishra, W. Cai, G. Tan, Materials Science in Semiconductor Processing 68, 58 (2017); https://doi.org/10.1016/j.mssp.2017.06.015

[2] A. M. Salema, M.O. Abou-Helal, Material Chemistry & Physics 80, 740 (2003); https://doi.org/10.1016/S0254-0584(03)00081-6

[3] A. Łapińska, A. Taube, M. Wąsik, G. Z. Żukowska, A. Duzynska, J. Judeka and M. Zdrojek,J. Raman Spectrosc. 48, 479 (2016); https://doi.org/10.1002/jrs.5064

[4] F. G. Hone, F. K. Ampong, Materials Chemistry and Physics 183, 320 (2016); https://doi.org/10.1016/j.matchemphys.2016.08.034

[5] K. T. Reddy, N. K Reddy, R.W. Miles, Solar Energy Materials and Solar Cells 90, 3041 (2006); https://doi.org/10.1016/j.solmat.2006.06.012

[6] L.P. Deshmukh, B. M. More, C.B. Rotti, G. S. Shashare, Materials Chemistry and Physics 45,145 (1996); https://doi.org/10.1016/0254-0584(96)80092-7

[7] A.K. Deb, V. Kumar, Physica Status Solidi B 254, 1600379-1, (2017); https://doi.org/10.1002/pssb.201600379

[8] T. A. Kuku, S.O. Azi, Journal of Materials Science 33, 3193 (1998); https://doi.org/10.1023/A:1004364310687

[9] B. Thangaraju, P. Kaliannan, Crystal Research Technology 35(1), 71 (2000); https://doi.org/10.1002/(SICI)1521-4079(200001)35:1<71::AID-CRAT71>3.0.CO;2-U

[10] S.A. Bashkirov, V. F.Gremenok, V.A. Ivanov, K. Bente, P. P. Gladyshev, T. Y. Zelenyak,Thin Solid Films 616, 773 (2016); https://doi.org/10.1016/j.tsf.2016.10.003

[11] A.Ishida, K. Matsushita, T. Sugimoto, H. Akimoto, S. Mohammadnejad, H. Fujiyasu,Surface Science 267, 149 (1992); https://doi.org/10.1016/0039-6028(92)91110-W

[12] G. F Hone, F. B. Dejene, O. K. Echendu, Surface Interface Analysis 2018, 1 (2018).

[13] U. Chalapathi, Y. Jayasree, S. H. Park, Materials Science in Semiconductor Processing 150,

106958-1 (2022); https://doi.org/10.1016/j.mssp.2022.106958

[14] U. Kumar, Y. Yang, Z. Y. Deng, M. W. Lee, W. M. Huang, C. H. Wu, Sensors and Actuators: B. Chemical 353, 131192-1 (2022); https://doi.org/10.1016/j.snb.2021.131192

[15] D. Lincot, Thin Solid Films 487, 40 (2005https://doi.org/10.1016/j.tsf.2005.01.032

[16] N. K. Reddy, K.T. R. Reddy, Solid-State Electron. 49, 902(2005); https://doi.org/10.1016/j.sse.2005.03.003

[17] G. G. Ninan, C. S. Kartha, K. P. Vijayakumar, Journal of Analytical and Applied Pyrolysis 120, 121(2016); https://doi.org/10.1016/j.jaap.2016.04.016

[18] L. Tzounis, M. Liebscher, F. Fuge, A. Leonhardt, V. Mechtcherine, Buildings 191, 151(2019); https://doi.org/10.1016/j.enbuild.2019.03.027

[19] Z. Zhang, Y. Wu, H. Zhang, Z. Zeng, Z. Hu, J Mater Sci: Mater Electron 26, 1619 (2015); https://doi.org/10.1007/s10854-014-2585-8

[20] E. Barrios-Salgado, M. T. S. Nair, P. K. Nair, Thin Solid Films 598, 149 (2016); https://doi.org/10.1016/j.tsf.2015.11.075

[21] S. R. S. Kumar, P. K. Nayak, M. N. Hedhili, M. A. Khan, H. N. Alsharee, Applied Physics Letters 103, 192109-1 (2013); https://doi.org/10.1063/1.4829356

[22] J. Damisaa, J. O. Emeghaa, I. L. Ikhioya, J. Nig. Soc. Phys. Sci. 3, 455 (2021); https://doi.org/10.46481/jnsps.2021.157

[23] M. Paal, I. Nkrumah, F. K. Ampong, D. U. Ngbiche, R. K. Nkum , F. Boakye, Science Journal of University of Zakho 8(3), 97 (2020); https://doi.org/10.25271/sjuoz.2020.8.3.752

[24] C. K. Bandoh, I. Nkrumah, F. K. Ampong, R. K. Nkum, F. Boakye, Chalcogenide Letters 18(2), 81 (2021).

[25] D. B. Puzer, I. Nkrumah , F. K. Ampong, M. Paal, E. A. Botchway, R. K. Nkum, F. Boakye, Chalcogenide Letters 18(8), 481 (2021).

[26] S. Sebastian, I. Kulandaisamy, S. Valanarasu, I. S. Yahia, H. Kim, D. Vikraman, Journal of Sol-Gel Science and Technology 93, 52 (2020); https://doi.org/10.1007/s10971-019-05169-y

[27] R. L. Orimi, H. K. Fadafan, A. Asadpour, European Physical Journal (Applied Physics)67, 20404-1 (2014); https://doi.org/10.1051/epjap/2014140159